

Turbulence signatures in high-latitude ionospheric scintillation

Meziane Karim¹, Hamza Abdelhaq M¹, and Jayachandran P. T.¹

¹University of New Brunswick

November 16, 2022

Abstract

Ground-based amplitude measurements of GNSS signal during ionospheric scintillation are analyzed using prevalent data analysis tools developed in the fields of fluid and plasma turbulence. One such tool is the structure function of order q , with $q = 1$ to $q = 6$, which reduces to the computation of the second order difference in the GPS signal amplitude at various time lags, and allows for the exploration of dominant length scales in the propagation medium. We report the existence of a range where the structure function is linear with respect to time lag. This linear time-segment could be considered as an analog to the inertial range in the context of neutral and plasma turbulence theory. Below the linear range, the structure function increases nonlinearly with time lag, again in good concordance with the intermittent character of the signal, given that a parallel is drawn with turbulence theory. Quantitatively, the slope of the structure function in the linear range is in good agreement with the scaling exponent determined from in-situ measurements of the electrostatic potential at low altitude (E-region) and the electron density at the topside ionosphere (F-Region). This in turn suggests the conjecture that scintillation could be considered a proxy for ionospheric turbulence. Furthermore, we have found that the probability distribution function of the second order difference in the signal amplitude has non-Gaussian features at large time-lags; a result that seems inconsistent with equilibrium statistical physics which suggests a Gaussian distribution for the conventional random walk processes.

1 **Turbulence signatures in high-latitude ionospheric**
2 **scintillation**

3 **K. Meziane¹, A. M. Hamza¹, and P. T. Jayachandran¹**

4 ¹Physics Department, University of New Brunswick, Fredericton, Canada.

5 **Key Points:**

- 6 • Evidence for the existence of a linear range in the the structure function of iono-
7 spheric scintillation
8 • The structure function slope in the linear range is consistent with the scaling ex-
9 ponent of the ionospheric electron density fluctuations
10 • Indications that the equilibrium state related to scintillation is dominated by non-
11 Gaussian statistics

Abstract

Ground-based amplitude measurements of GNSS signal during ionospheric scintillation are analyzed using prevalent data analysis tools developed in the fields of fluid and plasma turbulence. One such tool is the structure function of order q , with $q = 1$ to $q = 6$, which reduces to the computation of the second order difference in the GPS signal amplitude at various time lags, and allows for the exploration of dominant length scales in the propagation medium. We report the existence of a range where the structure function is linear with respect to time lag. This linear time-segment could be considered as an analog to the inertial range in the context of neutral and plasma turbulence theory. Below the linear range, the structure function increases nonlinearly with time lag, again in good concordance with the intermittent character of the signal, given that a parallel is drawn with turbulence theory. Quantitatively, the slope of the structure function in the linear range is in good agreement with the scaling exponent determined from in-situ measurements of the electrostatic potential at low altitude (E-region) and the electron density at the topside ionosphere (F-Region). This in turn suggests the conjecture that scintillation could be considered a proxy for ionospheric turbulence. Furthermore, we have found that the probability distribution function of the second order difference in the signal amplitude has non-Gaussian features at large time-lags; a result that seems inconsistent with equilibrium statistical physics which suggests a Gaussian distribution for the conventional random walk processes.

1 Introduction

Ionospheric scintillation is the physical phenomenon associated with distortions that arise in Global Navigation Satellite System (GNSS) radio wave fronts as they propagate through the ionosphere (Kintner et al., 2001). It is imputable to irregularities in ionospheric electron density, which arise from various plasma instabilities. As a consequence, structures in electron density form, which in turn affect the dielectric properties of the medium including its refractive index. Radio waves propagating through a structured ionosphere are scattered, and it is the signatures of various scattering processes that allow us to extract some of the fundamental ionospheric properties without in-situ measurements, a reverse engineering exercise. On the ground, a GNSS receiver records a time-series and reveals patterns which very much depend on the spatial and temporal conditions of the ionospheric medium through which the radio signal propagated. In other words, we ought to be able, through the principle of Inverse Scattering, to reconstruct some of the physical properties of the scattering medium. The scintillations recorded by the GNSS receiver hold integrated information about the ionospheric irregularities, their temporal and spatial scales, which can help narrow down the ionospheric plasma instability mechanisms at play. As an example, the equatorial anomaly (Groves et al., 1997) has long been understood as the cause of scintillation near the geomagnetic equator. In the ionospheric E and F regions, plasma instabilities such as the Farley-Buneman (Hamza & St-Maurice, 1993) and the gradient-drift are believed to be two of the most fundamental driving mechanisms that give rise to plasma density irregularities with characteristic length scales ranging from few centimetres to hundreds of kilometres (Aarons, 1982; Yeh & Liu, 1982; Wernik et al., 2007; Kintner et al., 2007). The size of these irregularities plays a central role when analyzing and especially when interpreting the data, which requires the knowledge to differentiate between refractive and diffractive signatures. Identifying the Fresnel field region and testing the Taylor frozen hypothesis to derive a temporal scale from the Fresnel scale are two of the most important steps in the interpretation of scattering data recorded by the GNSS receiver.

Empirically, scintillation studies use observables measured by GNSS receivers. Both signal's amplitude and phase are derived from the recorded measurements. For as long as lock is maintained between the satellite and the ground receiver, continuous measurements of the amplitude and phase can be recorded at usually a very high rate. When

64 the ray path (between the satellite orbiting at $\sim 20,000$ km from the centre of Earth)
 65 interacts with ionospheric irregularities, enhanced fluctuations rising above the background
 66 level in the signal's phase and amplitude appear. The conventional approach is to quan-
 67 tify the signal fluctuations using the scintillation indices S_4 and σ_ϕ indices correspond-
 68 ing to the variance of the amplitude and phase variations, respectively.

69
 70 The theoretical investigation of scintillation uses the wave equation as formulated
 71 for a random medium. An analytical closed form solution for the general case is not avail-
 72 able as the equation contains a stochastic parameter directly related to the density of
 73 scatterers. Approximations based on the nature of the interaction of the radio signal with
 74 the medium have been considered by several authors in order to derive the signal's elec-
 75 tric field. These models include the weak-scattering theory, the Rytov approximation and
 76 the phase screen theory based on a thin conducting layer approximation (Yeh & Liu, 1982;
 77 Priyadarshi, 2015). Under these models, ionospheric irregularity power spectra combined
 78 with the wave equation provide elements of comparison between theory and observations.

79
 80 In the present work, tools developed in the context of neutral fluid and plasma tur-
 81 bulence theories are used in order to unveil pertinent and dominant length scales respon-
 82 sible for ionospheric scintillation. This path has been initiated in a previous report in
 83 which intermittency was explored in ionospheric scintillation (Mezaoui et al., 2015); a
 84 statistical mechanics' approach, which analyzes the properties of fluctuations of the lo-
 85 cal variable measured, was used. These fluctuations tend to deviate from the homoge-
 86 neous and isotropic model of turbulence introduced by Taylor (1935, 1938), and have con-
 87 sistently been labeled as intermittent. This approach may be justified given that var-
 88 ious physical mechanisms can lead the ionospheric plasma to a turbulent state, partic-
 89 ularly when plasma instabilities evolve toward a nonlinear regime. Ionospheric plasma
 90 turbulence, driven by various instability mechanisms, which give rise to density irreg-
 91 ularities, often exhibit an electron density power spectrum with a power law qualitatively
 92 similar to the Kolmogorov (1941) power law for the velocity field in the context of fluid
 93 turbulence theory. The mathematical framework used in the present work is briefly de-
 94 picted in Section 2, while Section 3 describes the data. In Section 4, the results are pre-
 95 sented followed by a discussion section (Section 5).

96 2 The Structure Function

97 The fields of neutral fluid and plasma turbulence are mature research fields that
 98 have evolved for more than a century. A number of mathematical tools have been de-
 99 veloped to quantify and capture the underlying physical mechanisms responsible for the
 100 turbulent structure of the neutral fluid or the plasma, respectively. The statistical me-
 101 chanics approach consists of estimating ensemble properties that can be derived by coarse-
 102 graining the fields and studying the dependence of the fluctuations on the coarse-graining
 103 scales. This has led fluid dynamicists, for example, to study the probability distribution
 104 of the velocity increment $U(r + \delta) - U(r)$ instead of solving the Navier-Stokes equa-
 105 tion (Benzi et al., 1993), a nonlinear partial differential equation with no closed form so-
 106 lutions known in the case of turbulence; the probability distribution is then found to be
 107 skewed. Skewness would vanish only if there were invariance under time reversal, but
 108 for a turbulent dissipative flow this is not the case (for a mathematical proof, see (Lawrance,
 109 1991; Sosa-Correa et al., 2019)). This result has profound consequences since one is of-
 110 ten led to believe that the probability distributions ought to be normal or log-normal,
 111 which would imply a zero skewness, a result that is inconsistent with observations. As
 112 stated by the Nobel Prize laureate David Ruelle, "the lognormal theory contains an el-
 113 element of truth but has limited applicability" (<https://arxiv.org/abs/1405.5746>).

114 To illustrate the use of this statistical approach, we focus on the coarse-grained one-
 115 dimensional velocity fluctuations. One is then able to extend the method to the case of

116 plasma fluctuations, including the flow velocity fluctuations, the electric and magnetic
 117 field fluctuations or a combination. In this context, and in the fluid flow velocity $U(r)$
 118 case, the structure function of order q is defined as follows (Chang, 2015):

$$119 \quad D_q(\delta) = \langle |U(r + \delta) - U(r)|^q \rangle \quad (1)$$

120 where $\langle \rangle$ represents the ensemble average. In Expression (1), the difference of the flow
 121 speed U is between two points spatially separated by the scale δ . For simplicity, the struc-
 122 ture function $D_q(\delta)$ is formulated in the one dimensional case. The conventional anal-
 123 ysis consists of exploring the dependence of the structure function on the coarse-graining
 124 scale δ and the exponent index q . A turbulent system with a Kolmogorov scaling is con-
 125 sistent with a structure function in the form:

$$126 \quad D_q(\delta) \sim \delta^{\xi(q)} \quad (2)$$

127 Within the inertial range, where the equilibrium state is characterized by self-similarity
 128 and the power spectrum by a power law, the structure function $D_q(\delta)$ is supposed to re-
 129 main linear in δ independent of q . For the particular case of Kolmogorov turbulence, $\xi(q) =$
 130 $q/3$; in other words, the structure function of order 3 is $S_3 \sim \delta$. It is worth elaborat-
 131 ing on the Kolmogorov result, which is based on the suggestion by Obukov (1962) that
 132 the average rate of energy dissipation per unit mass $\langle \epsilon \rangle$ should be replaced by the spa-
 133 tially averaged dissipation defines as:

$$134 \quad \epsilon_\delta = \frac{1}{\delta} \int_{r_0}^{r_0+\delta} \epsilon(r) dr \quad (3)$$

135 Kolmogorov (1962) introduced a refined self-similarity hypothesis relating the structure
 136 functions for the flow velocity to the moments of the scale dependent rate of energy dis-
 137 sipation.

$$138 \quad D_q(\delta) = C_q \langle (\epsilon)^\frac{q}{3} \rangle \delta^\frac{q}{3} \quad (4)$$

139 The essential result of this hypothesis is that the statistics of $S_3(\delta)/\delta$ is the same as the
 140 statistics of ϵ_δ . In other words, the ratio $S_3(\delta)/\delta\epsilon_\delta$ is a random variable with a univer-
 141 sal distribution. A similar argument can be extended to higher order structure function
 142 by noting that $D_q(\delta) \sim D_3(\delta)^{\xi(q)}$, i.e., one is able to quantify the statistical properties
 143 of higher order structure function by knowing the statistics of the structure function of
 144 order 3. Note that below the inertial scale (dissipation scale), the linearity is violated.

145
 146 Empirically, the pertinence of turbulence methods requires in-situ multi-point mea-
 147 surements. In general, satellite observations of the terrestrial plasma environment are
 148 single-point time series measurements. In the interplanetary medium for example, satel-
 149 lites such as Wind and ACE are assumed to be nearly at rest with respect to the solar
 150 wind motion. In this context, the solar wind velocity and magnetic field measurements
 151 constitute data sets that enable to explore the validity of the Magnetohydrodynamic (MHD)
 152 approximation, and test plasma turbulence models of a natural system when certain phys-
 153 ical conditions are fulfilled. A number of extended studies of solar wind using turbulence
 154 have been reported (Carbone et al., 1997; Pagel & Balogh, 2002).

155 However, one should emphasize that in order to validate such studies one has to
 156 identify the limitations imposed by the fundamental assumptions based on single-point
 157 time series measurements. These assumptions include homogeneity and stationarity over
 158 the time range of interest. Under Taylor's frozen turbulence approximation, the struc-
 159 ture function at scale τ identifies an eddy at a scale length $\delta = U_0\tau$, where U_0 is the
 160 average speed over the time interval considered. The Taylor approximation allows us to
 161 define the structure function of order q as follows:

$$162 \quad S_q(\tau) = \langle |U(t + \tau) - U(t)|^q \rangle \quad (5)$$

163 where the ensemble average $\langle \rangle$ is now equivalent to a time average, given the assump-
 164 tion of stationarity.

165
 166 In the ionospheric context, turbulence is often triggered by various plasma insta-
 167 bilities giving rise to electron density fluctuations (Kintner et al., 1982). At low altitude
 168 (E-region) where the collisional effects between the ionospheric plasma and the upper
 169 neutral atmosphere are important, the two-stream (Farley–Buneman) instability is of-
 170 ten excited (Farley, 1963; Buneman, 1963) as the main mechanism for the development
 171 of electron density irregularities. In the F-region both the gradient-drift and Kelvin-Helmholtz
 172 instabilities occur. Various studies revealed that ionospheric plasma structuring, such
 173 as sporadic E-layer or the trailing edge of polar cap patches, result from the gradient-
 174 drift and Rayleigh-Taylor instabilities (Sato et al., 1968). Ionospheric turbulence is now
 175 well established and the inherent mechanisms are well documented in the literature (Kintner
 176 & Seyler, 1985). Several studies investigated the turbulent features related to the iono-
 177 spheric electric field, electron density and magnetic field at various latitudes (Hamza &
 178 St-Maurice, 1993; Dyrud et al., 2008). The non-linear development of plasma irregu-
 179 larities and the energy cascade from large to small scales lead to power spectra of electron
 180 density fluctuations that are well fitted by a power law (Mounir et al., 1991). This shape
 181 of the power spectral density pinpoints to scale invariance similar to what was developed
 182 in fluid turbulence theory. An important consequence of the ionospheric turbulence is
 183 its impact on the propagation of radio wave signals emitted by Global Navigation Satel-
 184 lite Systems (GNSS). Our main interest lies in the identification of scaling arguments
 185 in the scintillation data that are conformal to the arguments used to characterize iono-
 186 spheric turbulence. By analogy, we will analyze the time series of the signal amplitude
 187 measured, at a single point, by a GNSS receiver assuming conditions similar to those of
 188 Kolmogorov turbulence, namely stationarity, homogeneity and isotropy. We will com-
 189 pute the structure functions and study their dependence on time lag τ . In principle, it
 190 is assumed that a radio wave front, propagating through a turbulent ionospheric layer,
 191 will be significantly altered, and the distortions strongly linked to the presence of elec-
 192 tron density irregularities.

193 The present analysis requires the assumption of stationarity of the scintillation time
 194 series. While this condition is difficult to establish, it is reasonable to assume that the
 195 recorded signal is locally stationary if the scintillation time interval is measured over a
 196 short duration. Previous studies have indicated that the lifetime of large-scale density
 197 gradients exceeds several times the time scale for linear growth of the gradient drift in-
 198 stability (Basu et al., 1990). The Taylor hypothesis is now examined in the context re-
 199 lated to the study carried out on amplitude scintillation. On the ground, the measured
 200 signal results from the propagation of a radio wave as it propagates through a moving
 201 ionospheric plasma. The theoretical determination of the scan velocity (V_{eff} , for effec-
 202 tive velocity) is a complex problem as it depends upon the satellite motion, the irreg-
 203 ularity drift motion as well as the anisotropy of the irregularity with respect to the geo-
 204 magnetic field. Assuming a model of irregularity in which the electron density variance
 205 is distributed according to a spheroid, several authors attempted to estimate V_{eff} (Rino,
 206 1979; Carrano et al., 2016). Under some conditions at low-latitude, Carrano et al. (2016)
 207 derived the following approximation for V_{eff} :

$$208 \quad V_{eff} \sim 1.11 \frac{\sigma_{\Phi}}{S_4} \rho_F \quad (6)$$

209 where S_4 and σ_{Φ} are the amplitude scintillation and phase variation indices, and ρ_F the
 210 first Fresnel zone radius with $\rho_F^2 = \frac{z\lambda}{2\pi \cos \theta}$ in which λ is the carrier wavelength, z is the
 211 height of the scattering layer and θ the angle between the zenith and the direction of mo-
 212 tion of the emitting satellite. For a high elevation angle and assuming the scattering layer
 213 is located within the F-region (~ 300 km), the corresponding L-band effective scan ve-
 214 locity $V_{eff} \sim 100 \frac{\sigma_{\Phi}}{S_4}$. Based on numerous index measurements, it is reasonable to con-
 215 sider that a rule of thumb $\frac{\sigma_{\Phi}}{S_4} \sim 1-2$ (Ghobadi et al., 2020) yielding an estimation of
 216 V_{eff} in the 100 – 200 m/s range. In order for the Taylor hypothesis to hold, the scan

217 speed should remain significantly smaller than the speed of any changes affecting the ir-
 218 regularity. To be more specific, Taylor’s hypothesis postulates a linear relationship, non-
 219 dispersive, between frequency and wavenumber, $\omega' = \omega + kV_0 \simeq kV_0$, where V_0 is the
 220 velocity of the plasma turbulent flow over the detector, ω' (ω) is the measured (plasma
 221 rest) frequency. In principle, if one identifies V_0 with V_{eff} , then one would require a large
 222 effective velocity for Taylor’s hypothesis to remain valid.

223
 224 Moreover, we assume that the ionospheric turbulence, with a measured power spec-
 225 trum, is driven by instability mechanisms that allow the development of density struc-
 226 tures, which in turn act as random scatterers (Rufenach, 1972). The analogy consists
 227 of treating the recorded radio signal by the GNSS receiver as similar to the to single-point
 228 measurement of the flow velocity in a turbulent medium that can be modelled using the
 229 Kolmogorov (1962) model (Falcon, 2010). Wave turbulence in the terrestrial plasma en-
 230 vironment has been addressed theoretically (Sagdeev, 1979) as well as from the obser-
 231 vations point of view.

232 Under the conditions described above, for a time series of the signal amplitude $u(t)$,
 233 the turbulence estimator is defined in a similar way as:

$$234 \quad S_q(\tau) = \langle |u(t + \tau) - 2u(t) + u(t - \tau)|^q \rangle \quad (7)$$

235 where $\langle \rangle$ represents time averages. Note that the expression between bracket is related
 236 to the second time derivative of the amplitude $u(t)$ for small lag-times.

$$237 \quad \frac{d^2u(t)}{dt^2} = \lim_{\tau \rightarrow 0} \frac{1}{\tau^2} [u(t + \tau) - 2u(t) + u(t - \tau)] \quad (8)$$

238 The choice of the structure function expression (7) rather than expression (5), although
 239 not fundamental, is justified according to the following argument. The analogy between
 240 wave turbulence and fluid turbulence remains limited as the underlying governing equa-
 241 tions are different. Fluid turbulence is caused by the presence of viscous forces that lead
 242 to relative motions within the fluid. Relative motions can also be produced by the in-
 243 jection of high or low streams inside the fluid. On the other hand, wave turbulence arises
 244 from the nonlinear interaction of waves excited through instability mechanisms. Initially
 245 of small amplitude, waves excited through instabilities undergo further growth reaching
 246 large enough amplitudes to nonlinearly interact with the background flow and other waves
 247 within the emitted spectrum; this in turn will lead to saturation if a stationary equilib-
 248 rium is possible. The nonlinear interaction of waves leads to a distribution of power over
 249 spatial and temporal scales that can be modelled, under some important assumptions,
 250 by Kolmogorov-like power laws (cascade models). Moreover, one important feature of
 251 fluid turbulence is intermittency, which results from bursts of intense motion that are
 252 produced and dominated by small scale structures. Therefore, intermittent systems are
 253 characterized by non-Gaussian probability density functions imputed to the formation
 254 of vortices. In wave turbulence, however, the intermittency is often due to low wave num-
 255 ber Fourier amplitude (Choi et al., 2005), not necessarily related to hydrodynamics tur-
 256 bulence. While fluid turbulence is driven by the equation of motion, which involves the
 257 first time derivative of U , the wave turbulence is rather governed by the wave equation,
 258 which contains the second-time derivative of the wave amplitude. In the former case, the
 259 structure function is consistent with Expression (5), while in the latter case, it is con-
 260 form with Expression (7).

261 3 Scintillation data

262 GPS amplitude measurements used in the present study are from the Canadian High
 263 Arctic Ionospheric Network (CHAIN) (Jayachandran et al., 2009). With 28 GISTM re-
 264 ceivers and 9 ionosondes, the network’s coverage expands over Canada northern region.

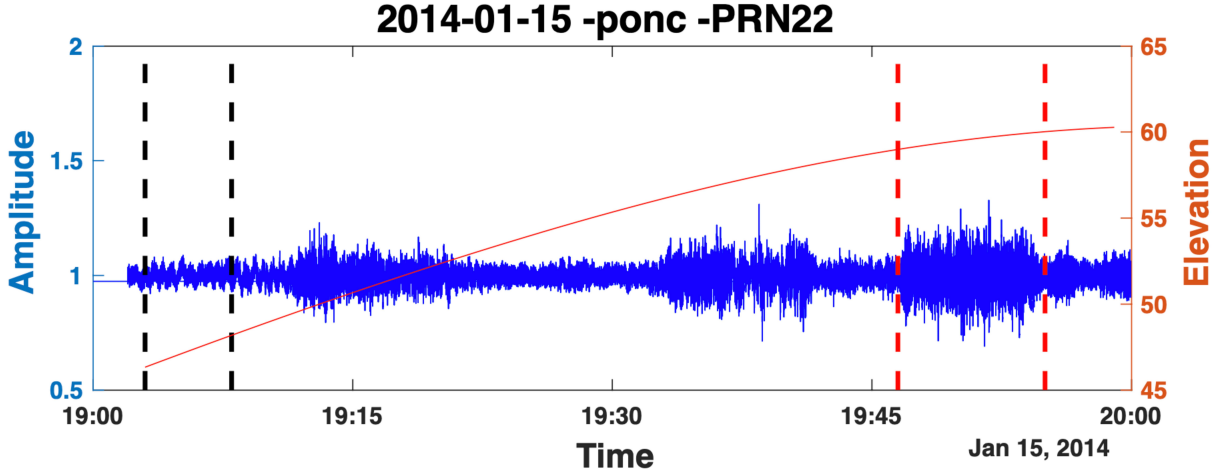


Figure 1. Time series of the amplitude scintillation recorded on January 15, 2014, 1900-2000 UT at *Pond-Inlet* station and from PRN 22. The red continuous line indicates the satellite elevation angle. The red (black) dashed vertical bars mark the time interval of the analyzed event (background).

265 Data collected by the receivers located at *Pond-Inlet*, (*ponc*) Magnetic Coordinates =
 266 (82.3°N, 2.6°E) and *Arctic Bay* (*arcc*) Magnetic Coordinates = (82.1°N, 27.0°E) are of
 267 interest in the present work; both stations are located in the statistical cusp region. One
 268 should mention that the selection of these 2 stations is not dictated by any physical con-
 269 sideration except by the good quality of data at these stations. Both stations *ponc* and
 270 *arcc* operate with high rate GNSS measurements at 50 Hz. In order to eliminate effects
 271 due to satellite motion, a detrending operation using a standard sixth order Butterworth
 272 filter with a cutoff frequency of $f_c = 0.1$ Hz was applied to the signal prior to any anal-
 273 ysis (Mushini, 2012). Given the PRN high elevation angle associated with the events stud-
 274 ied below, it is unlikely that these events result from multi-path. In addition, with the
 275 same PRNs, no amplitude fluctuations level above the background are noticed prior and
 276 after one sidereal day the time of interest. Therefore, the possibility that events analyzed
 277 below result from multi-path is ruled out as it is assured that they correspond to scin-
 278 tillation of ionospheric origin.

279 4 Results

280 4.1 2014 January 15 event

281 Figure 1 shows the L1 signal amplitude of PRN number 22 and recorded by a GPS
 282 receiver located at *ponc* station on January 15, 2014, 1900 – 2000 UT. The selected in-
 283 terval reveals time segments where amplitude fluctuations are enhanced (1911-1918 UT,
 284 1921-1942 UT, 1946-1955 UT) comparatively to others corresponding to the receiver back-
 285 ground level (1903-1908 UT). It is believed that these enhanced fluctuations result from
 286 scattering of the radio signal propagating through Fresnel scale ionospheric structures.
 287 The continuous red curve indicates the elevation angle of the ray path during the hour.
 288 The analysis sequence is now carried out on the time segment marked by the two red
 289 vertical bars, i.e. 1946–1955 UT interval where the amplitude fluctuations appear the
 290 highest during the hour. In comparison, the two black vertical bars indicate a selected
 291 time interval for the receiver background (1903–1908 UT). We mention that the year
 292 2014 corresponds to a near solar maximum activity phase in which ionospheric scintil-
 293 lation occur more frequently (Akala et al., 2011; Meziane et al., 2020). The structure func-

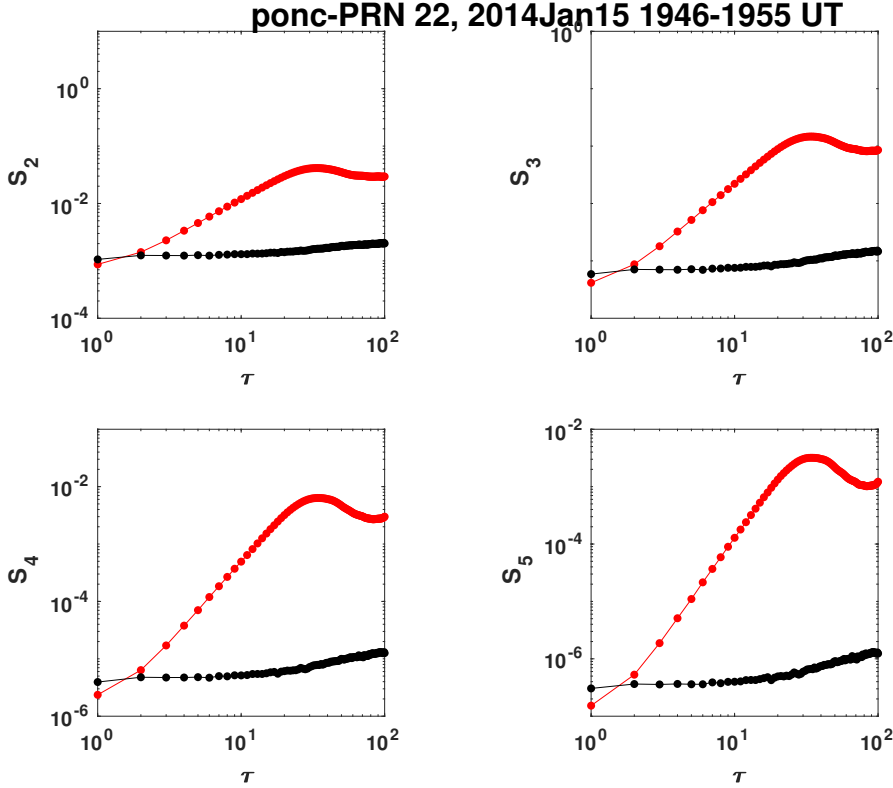


Figure 2. In red, the structure function for $q = 2, 3, 4, 5$ is plotted versus the time scale τ for the time interval 1946 – 1955 UT on 2014 January 15 at *Pond-Inlet* station. The same computation is undertaken in absence of scintillation and the result is represented by the plot in black.

294 tions of order $q = 1$ to $q = 6$ are now empirically calculated at various time scale τ
 295 using scintillation data collected by CHAIN. At this time, we contemplated that no valu-
 296 able information is gleaned for numerical values of $q > 6$. Figure 2 shows the variation
 297 of the structure function S_q (Expression 7) for $q = 2, 3, 4, 5$ versus the time scale τ taken
 298 over a continuous interval. A common feature, the shape of the structure function, is re-
 299 vealed for all values of q considered. A similar pattern is obtained for $q = 1$ and $q =$
 300 6 (not shown). While the red plot represents the scintillation event, the back curve cor-
 301 responds to the receiver background signal for which S_q is also computed. For clarity
 302 and in order to display the quantitative feature of S_q for various q , the same y -axis limit
 303 range is set. Qualitatively, a similar trend appears for all q index values. While S_q for
 304 the receiver background signal is found to be nearly independent of the time-scale τ , it
 305 exhibits a characteristic signature when ionospheric scintillation is present. In particu-
 306 lar, we note that for all values of the q index there exists a range $\Delta\tau$ for which the struc-
 307 ture function is linear in τ , $S_q \sim \tau^{\xi(q)}$ (the plots on Figure 2 are in log-log scale). In
 308 this particular case, Figure 2 clearly shows that the slope $\xi(q)$ increases with q . In order
 309 to precisely identify the range $\Delta\tau$ over which S_q is linear in τ , the derivative of S_q
 310 with respect to τ is numerically computed by taking the difference $\Delta S_q(\tau)$ of the struc-
 311 ture function between two adjacent points, i.e. $\Delta S_q(\tau) = S_q(\tau + 1) - S_q(\tau)$. Figure 3
 312 shows the obtained results. As shown on this last figure, the variations of $\Delta S_q(\tau)$ dis-
 313 plays three distinct ranges. First, a prevailing range where $\Delta S_q(\tau)$ plateaus according
 314 to a numerical value that increases with q . A close inspection indicates that this range
 315 is established between $\tau = \tau_1 = 3$ and $\tau = \tau_2 = 15$, corresponding to times $t_1 = 0.06s$
 316 and $t_2 = 0.30s$. Below the time scale τ_1 , the linearity of the structure function is not

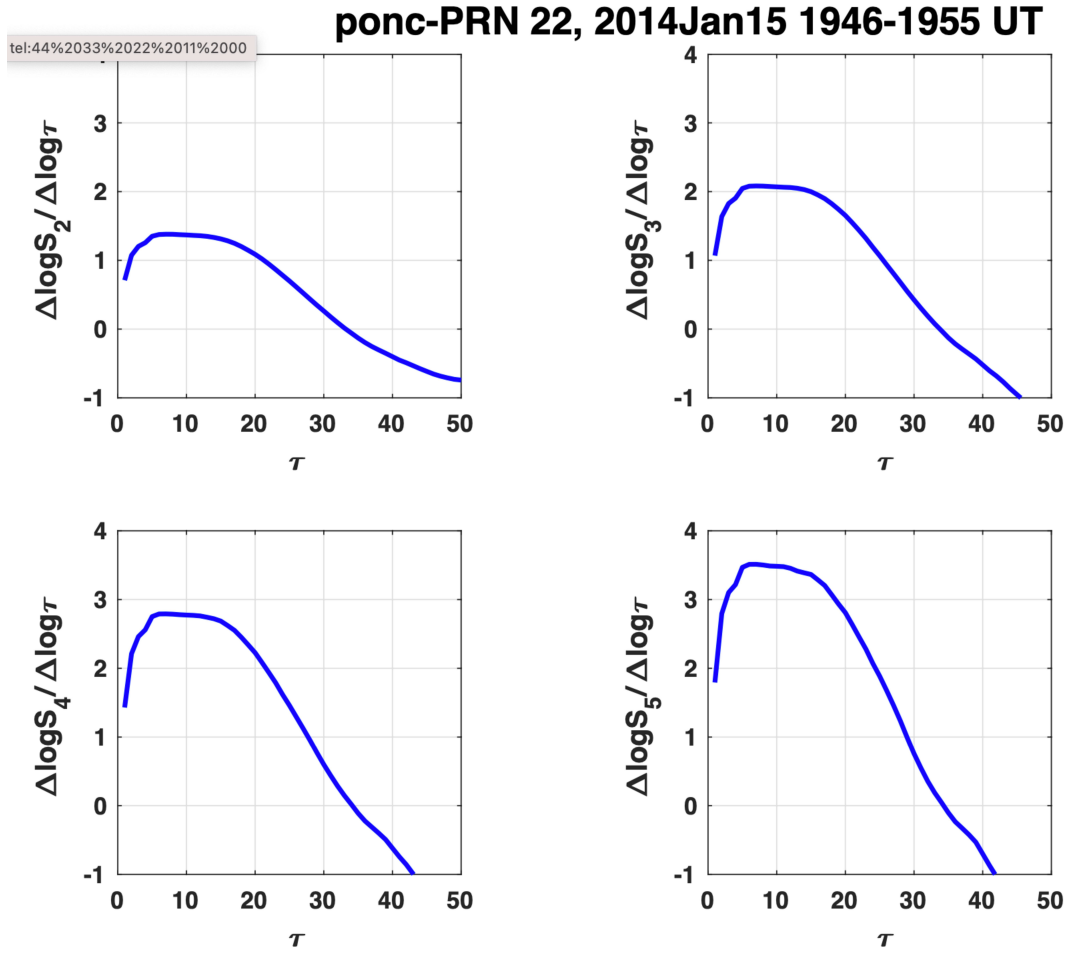


Figure 3. Variation of the difference $\Delta S_q(\tau) = S_q(\tau + 1) - S_q(\tau)$ versus τ for various values of q -index.

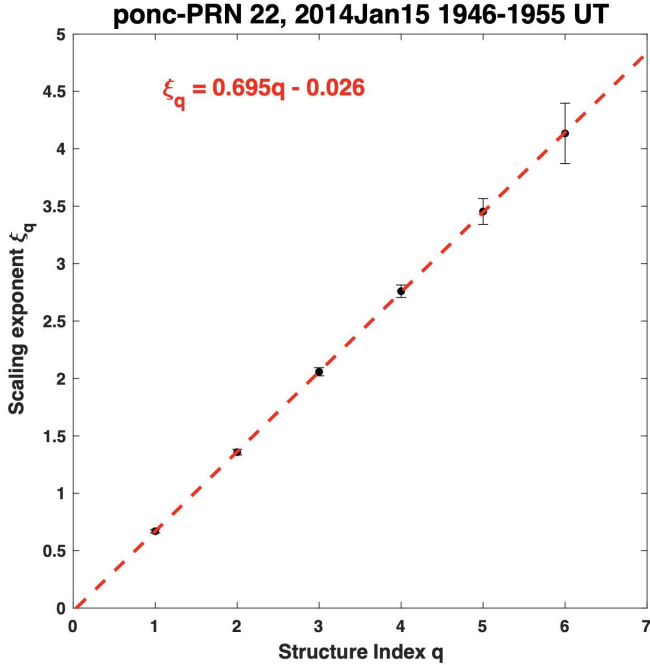


Figure 4. Scaling component ξ_q versus q -index within the range. The red dashed line represents the best linear fit.

317 validated, while for $\tau > \tau_2$ the linearity is broken and the structure function seems to
 318 reach a saturation level. To complete the analysis, it is instructive to examine the nu-
 319 merical values for the scaling component $\xi(q)$ in terms of q . The obtained results are shown
 320 on Figure 4, which clearly indicate that the scaling component in the range is $\xi(q)/q \approx$
 321 0.695. Further exploration of the shape of the distribution across the time scale τ is ex-
 322 amined in the next event.

323 4.2 2016 October 14 event

324 The same analysis, as performed above, is now carried out with a second scintil-
 325 lation event recorded at *Arctic Bay (arcc)* station on October 14, 2016, in 1723–1728
 326 UT interval indicated by the two red-dashed vertical bars shown on Figure 5. Also, the
 327 two black dashed vertical bars mark the considered receiver background fluctuations level
 328 in absence of scintillation (1732–1742 UT). The treatment of a supplementary event
 329 with similar qualitative result may appear redundant. Nevertheless, the exposition of the
 330 event has the purpose to evidence the existence of a linear range in the ionospheric func-
 331 tion for ionospheric scintillation. Again, the structure function (Expression 7) as a func-
 332 tion of time lag τ is computed for various values of q for both the selected intervals for
 333 the scintillation event and the background signal amplitude fluctuations; the result is shown
 334 on Figure 6. The presence of a linear range is evident for all values of q shown. A ju-
 335 dicious inspection yields an inertial range between $\tau_1 = 30$ and $\tau_2 = 40$ (0.6–0.8 sec
 336 range) with a scaling component $\xi(q)/q \approx 1.1$, significantly higher when compared to
 337 the one obtained for the January 17, 2014 event.

338
 339 The structure function at scale τ examined above is related to the moments of the
 340 distribution function of the second order difference in the signal amplitude $\eta(t) = u(t+$
 341 $\tau) - 2u(t) + u(t-\tau)$, where $u(t)$ is the scintillation amplitude. The global shape of the
 342 distribution density is reflected in the variation of the structure function as exhibited on
 343 Figure 2 and Figure 6. The distribution of $\eta(t)$ across the scales for few selected increas-

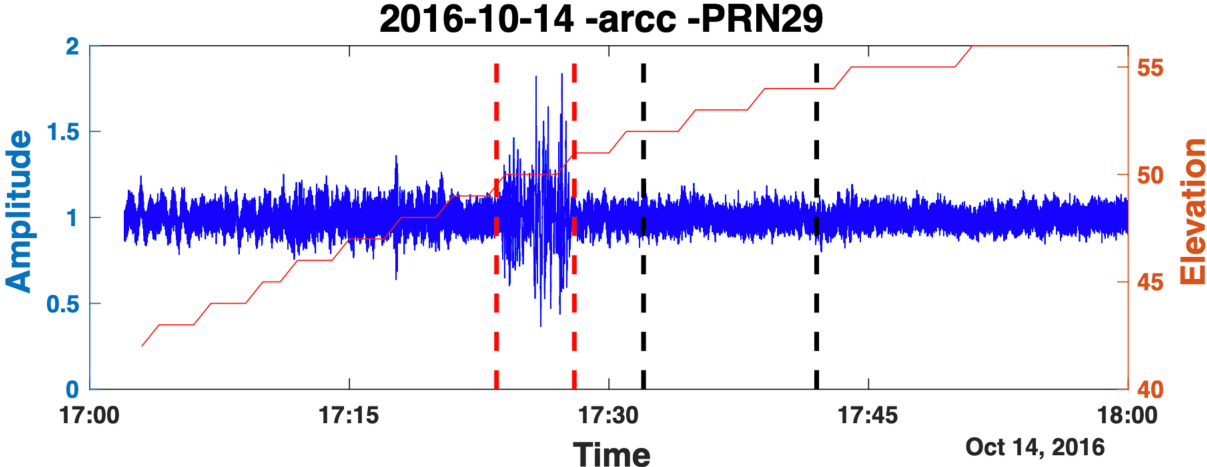


Figure 5. Time series of the amplitude scintillation recorded on October 14, 2016, 1700-1800 UT at *Arctic Bay* station and from PRN 29. The red continuous line indicates the satellite elevation angle. The red (black) dashed vertical bars mark the time interval of the analyzed event (background).

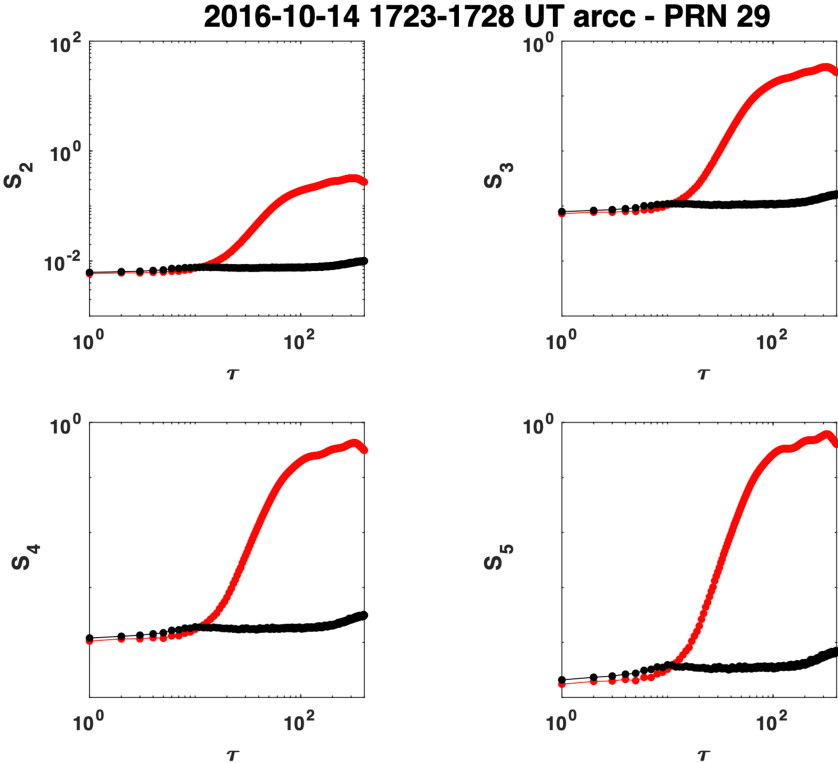


Figure 6. In red, the structure function for $q = 2, 3, 4, 5$ is plotted versus the time scale τ for the time interval 1732 – 1728 UT on 2016 October 14 at *Arctic Bay* station. The same computation is undertaken for the receiver background signal and the result is represented in black in the various plots.

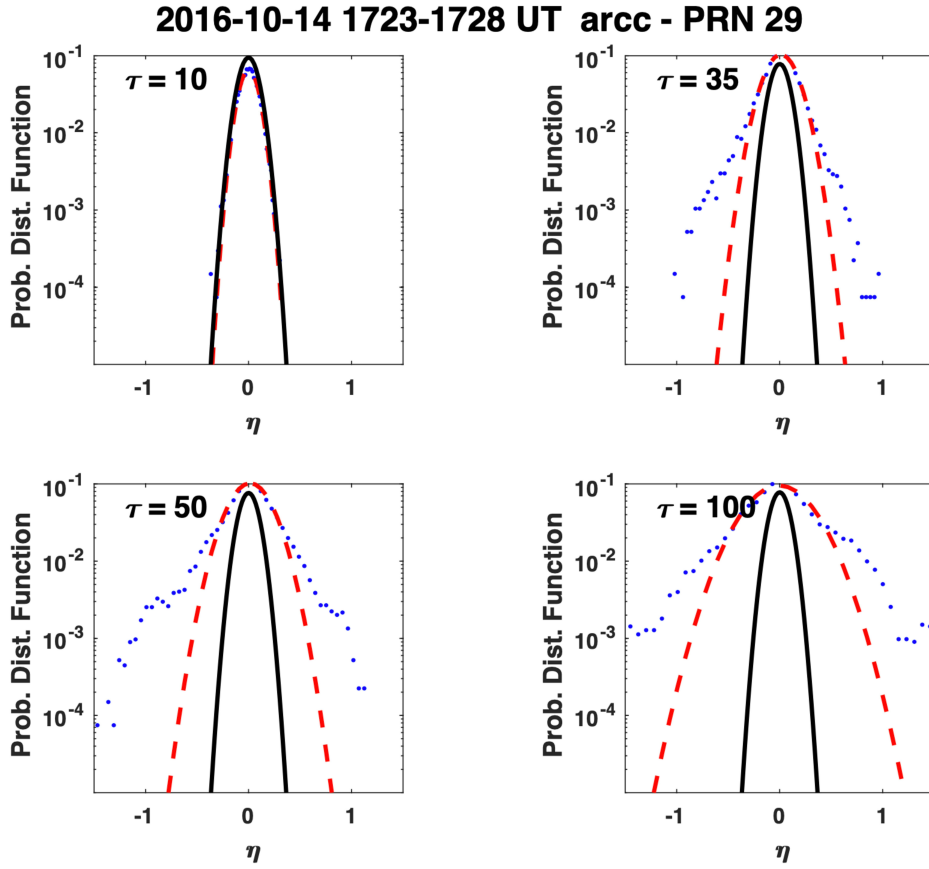


Figure 7. The blue dots represent the measured probability distribution function of $\eta(t)$ for time lags $\tau = 10, 35, 50, 100$ associated with the event interval indicated by the figure title. The red-dashed line corresponds to the best Gaussian fit to the measurement while the black continuous curve shows the distribution when no scintillation is present (background).

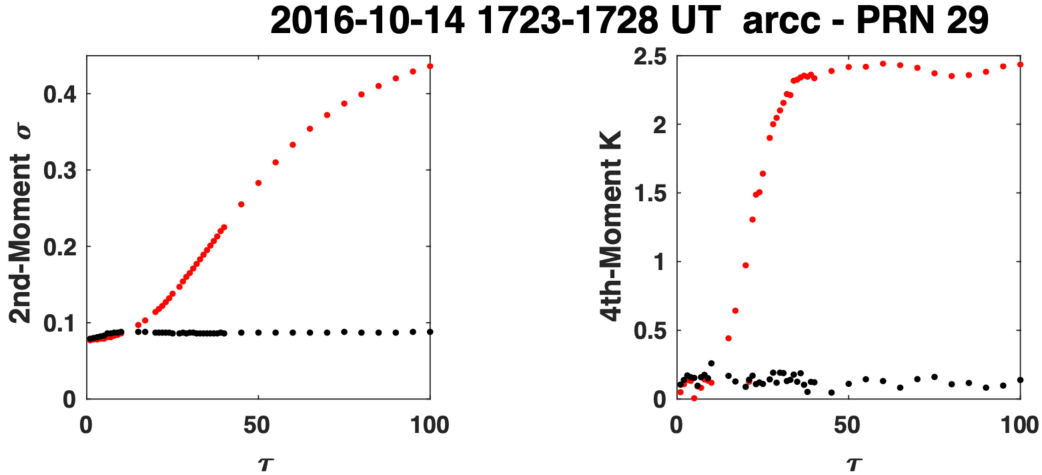


Figure 8. Second moment of distribution (left panel) and excess kurtosis (right panel) of $\eta(t)$ versus the time lag τ . The red dots correspond to the scintillation event while the black dots represent the background noise.

ing values of τ is shown on Figure 7. While the measurements are represented by the blue marks, the dashed red line corresponds the best Gaussian fit to the data. At the same time, the probability density of $\eta(t)$ fluctuations in the absence of scintillation is given by the continuous black curve. Clearly, the receiver background probability density remains invariant, while in the case of scintillation event the distribution undergoes a continuous widening departing from the Gaussian shape at higher scales. The peak of the distribution is satisfactorily fit using a Gaussian, but the emerging tails with increasing scale τ cannot be captured with Gaussian statistics. Departures from Gaussian statistics are usually quantified by distribution moments with orders higher than 2. In particular, the relevance of the tail is captured by the excess kurtosis ($= 0$ for a Gaussian). Panels on Figure 8 show the computed second (left panel) and fourth moments (right panel) of $\eta(t)$ for increasing scale τ , respectively. The red (black) marks correspond to numerical values obtained for the scintillation event (receiver background). Clearly, for the background signal, the computed moments appear insensitive to changes of τ and the excess kurtosis remains near a zero value as it is expected of a Gaussian process. On the contrary, for the scintillation event both moments increase with τ before reaching an asymptotic limit ($K \approx 2.4$). It is remarkable that the kurtosis K attains the asymptotic value at $\tau \approx 40$, basically the upper bound of the linear range.

5 Discussion and Conclusion

Analysis methods developed in the context of neutral fluid and plasma turbulence theory are adopted to explore the pertinent spatio-temporal scales in ionospheric scintillation physics. A justification of the approach is based on the consideration that ionospheric scintillation is produced when the radio signal propagates through a non-homogeneous medium undergoing at the same time spatio-temporal fluctuations. We have computed the structure function of order q , defined in our case as a second order difference in the signal amplitude at temporal scale τ is computed for various orders q . Qualitatively and through the perspective of fluid turbulence, the resulting variations of S_q as a function of τ are analogous to the numerical findings in Navier-Stokes turbulence (Benzi et al., 1993; Grossmann et al., 1997), wave turbulence (Falcon, 2010), and empirical results such those related to the solar wind turbulence (Carbone et al., 1997; Pagel & Balogh, 2002; Weygand et al., 2006). From the variations of S_q emerges a linear range analog to the

375 inertial range of fluid turbulence. Below the linear range, the linearity of the the struc-
 376 ture function is not satisfied, which seems to pinpoint to a dissipation range counterpart.
 377 The obtained scaling component value, which is event-dependent, is larger than the value
 378 found in Kolmogorov's turbulence ($\xi_3 > \xi_3^{(Kol)} = 1$). The essence of our study of higher
 379 order structure functions is to try and identify patterns in their behaviours with time
 380 delay like those found in the first, second and third order structure functions. The re-
 381 current linear behaviour with time delay is present in all the structure functions stud-
 382 ied up to order 6. As mentioned above, the relationship $S_q \sim S_3^{\xi(q)}$ explains this char-
 383 acteristic (when considering the log of the structure functions). Within the ionospheric
 384 plasma, the structure function has been previously constructed by means of numerical
 385 simulations and in-situ measurement in order to unveil the precise scaling features re-
 386 lated to ionospheric turbulence. Specifically, the electrostatic potential in the E-region
 387 (Dyrud et al., 2008) and electron density at the topside F-layer (De Michelis et al., 2021)
 388 provide the pertinent physical quantities for the analysis. For the electrostatic fluctu-
 389 ations, the structure functions for various q , and captured at a fixed point, increase with
 390 time lag and exhibit a linear range. At the same time, the probability density for the
 391 potential fluctuations follow a nearly Gaussian distribution. Furthermore, the numer-
 392 ical values obtained for the scaling exponents, when compared to those derived from rocket
 393 data based on two-point measurements, appear noticeably smaller (Dyrud et al., 2008).
 394 Nevertheless, the empirical determination of the scaling component appear similar to the
 395 scintillation equivalent linear range in the case $q = 1 - 4$. More recently, in a study
 396 reported by De Michelis et al. (2021), the scale invariance associated with ionospheric
 397 electron density fluctuations has been empirically investigated. The authors used in-situ
 398 1 Hz rate electron density measurements from the ESA-Swarm A satellite to evidence
 399 the existence of an inertial scale range associated with the plasma turbulence at the top-
 400 side ionosphere. In the cusp region, De Michelis et al. (2021) found that the first-order
 401 ($q = 1$) scaling exponent numerical value is comparable to the one obtained from the
 402 scintillation data analyzed in the present study. This concordance strongly indicates that
 403 the scaling features present in the ionospheric electron density fluctuations coherently
 404 echo in scintillation seen on the ground. Particularly, scintillation may possibly be con-
 405 sidered as a proxy for ionospheric turbulence. The extension of the present study to a
 406 larger collection of scintillation events could precise this aspect. Below the linear range,
 407 it is found that the structure function increases with time lag τ , a feature similar found
 408 in wave turbulence theory. In fluid turbulence, the dissipation region is dominated by
 409 enhanced fluctuations of short durations. This feature, commonly called intermittency,
 410 is also observed in wave turbulence. A scrutiny of the distribution function of fluctua-
 411 tions of the variable of interest in the intermittent region exhibits strong departure from
 412 the conventional Gaussian statistics. While the distribution function remains nearly sym-
 413 metric (skewness ~ 0), it reveals at the same time pronounced tails of flatness with a
 414 positive residual kurtosis (leptokurtic distribution). The bending of the structure func-
 415 tion, when the time scale τ is larger than the linear range, suggests that amplitudes in
 416 the signal separated by a long time-lag tend to be uncorrelated; no long time memory.
 417 One therefore expects Gaussian statistics for long-time scales. In other words, while all
 418 odd moments of the distribution of $\eta(t)$ vanish, the standardized even moments have fixed
 419 numerical values independent of the variance. Particularly, the excess kurtosis (fourth
 420 moment distribution) at large τ is close to zero. These results have been established the-
 421 oretically and empirically for both fluid and wave turbulence (Falcon, 2010), respectively.
 422 This picture is associated with diffusion processes and derived from the solutions of Fokker-
 423 Planck or Langevin equations.

424
 425 The results reported in the present work seemingly contrast with the prediction of
 426 a Gaussian closure as indicated by the non-zero asymptotic value of the residual kurtosis.
 427 The scattered radio signal through the ionosphere seems to be related to processes
 428 that are not fully uncorrelated over a range of length scales. A random-walk interpre-
 429 tation of the results suggests a wave-scattering process leading to non-Gaussian signa-

430 tures that arise when the steps of the walker happen to be correlated in a hierarchical
 431 way. Therefore, a proper and adequate understanding of the reported results, which need
 432 to be extended to include a larger data base in addition to a parametric study, requires
 433 the adoption of non-Gaussian models. A possible solution consists of exploring the scal-
 434 ing exponent for various geomagnetic conditions, and its latitude-dependence as well as
 435 an eventual association with the amplitude index S_4 . Such non-Gaussian models, among
 436 others, that are related to wave propagation through non-homogeneous media have been
 437 previously highlighted (Jakeman & Tough, 1988). In this respect, a model based on K -
 438 distribution that describes the amplitude of scattered waves through a rough surface seems
 439 to have attractive features as it provides practical statistical properties that could be ex-
 440 amined within the ionosphere context. Indeed, drawing a parallel between a structured
 441 ionospheric layer and an object with a rough surface can be very instructive when one
 442 considers the scattering of a radio wave by the ionosphere and the scattering of light by
 443 a rough surface. The emerging pattern from laser scattering by a rough surface is anal-
 444 ogous to the scintillation pattern observed when a radio wave propagates through a struc-
 445 tured ionosphere dominated by Fresnel-size scatterers. The analogy suggests a strong
 446 role played by diffraction in the production of ionospheric scintillation (McCaffrey & Jay-
 447 achandran, 2019). This path of studying the scintillation pattern through the lens of the
 448 diffraction by a rough object surface lies beyond the scope of our investigation.

449 Acknowledgments

450 CHAIN data are available through <http://www.chain-project.net/data/gps/data/raw/ponc/2014/01/>
 451 website. Infrastructure funding for CHAIN was provided by the Canadian Foundation
 452 for Innovation and the New Brunswick Innovation Foundation. CHAIN operations are
 453 conducted in collaboration with the Canadian Space Agency. This research was under-
 454 taken with the financial support of the Canadian Space Agency FAST program and the
 455 Natural Sciences and Engineering Research Council of Canada.

456 References

- 457 Aarons, J. (1982). Global morphology of ionospheric scintillations. *IEEE Proceed-*
 458 *ings*, *35*, 360–378.
- 459 Akala, A. O., Doherty, P. H., Valladares, C. E., Carrano, C. S., & Sheehan, R.
 460 (2011). Statistics of GPS scintillations over south america at three levels of
 461 solar activity. *Radio Sci.*, *46*, RS5018. doi: 10.1029/2011RS004678
- 462 Basu, S., Basu, S., MacKenzie, R., Coley, W. R., Sharber, J. R., & Hoegy, W. R.
 463 (1990). Plasma structuring by the gradient drift instability at high latitudes
 464 and comparison with velocity shear driven processes. *J. Geophys. Res.*, *95*,
 465 7799-7818.
- 466 Benzi, R., Ciliberto, S., Tripicciono, R., Baudet, C., Massaioli, F., & Succi, S.
 467 (1993). Extended self-similarity in turbulent flows. *Phys. Rev. E*, *48*, 29–
 468 32.
- 469 Buneman, O. (1963). Excitation of field aligned sound waves by electron streams.
 470 *Phys. Rev. Lett.*, *10*, 285.
- 471 Carbone, E., Bruno, R., & Veltri, P. (1997). Evidences for extended self-similarity in
 472 hydromagnetic turbulence. *Geophys. Res. Lett.*, *23*, 121–124.
- 473 Carrano, C. S., Groves, K. M., Rino, C. L., & Doherty, P. H. (2016). A technique
 474 for inferring zonal irregularity drift from single station gnss measurements of
 475 intensity (S_4) and phase (σ_Φ) scintillations. *Radio Sci.*, *51*, 1263–1277. doi:
 476 10.1002/2015RS005864
- 477 Chang, T. T. S. (2015). Probability distribution and structure functions. In
 478 *An introduction to space plasma complexity* (pp. 75–88). Cambridge University
 479 Press. Retrieved from <https://doi.org/10.1017/CBO9780511980251> doi: 10
 480 .1017/CBO9780511980251

- 481 Choi, Y., Lvov, Y. V., Nazarenko, S., & Pokorni, B. (2005). Anomalous probability
482 of large amplitudes in wave turbulence. *Phys. Lett. A*, *339*, 361–369.
- 483 De Michelis, P., Consolini, G., Pignalberi, A., Tozzi, R., Coco, I., Giannatta-
484 sio, F., ... Balasis, G. (2021). Looking for a proxy of the ionospheric
485 turbulence with swarm data. *Nature Scientific Reports*, *11*, 6183. Re-
486 trieved from <https://doi.org/10.1038/s41598-021-84985-1> doi:
487 10.1038/s41598-021-84985-1
- 488 Dyrud, L., Krane, B., Oppenheim, M., Pécseli, H. L., Trulsen, J., & Wernik,
489 A. W. (2008). Structure functions and intermittency in ionospheric plasma
490 turbulence. *Nonlin. Processes Geophys.*, *15*, 847–862. Retrieved from
491 www.nonlin-processes-geophys.net/15/847/2008/
- 492 Falcon, E. (2010). Laboratory experiments on wave turbulence. *Discrete and Con-
493 tinuous Dynamical Systems, Series B*, *13*, 919–940. doi: 10.3934/dcdsb.2010
494 .13.819
- 495 Farley, D. T. (1963). Two-stream plasma instability as a source of irregularities in
496 the ionosphere. *Phys. Rev. Lett.*, *10*, 279.
- 497 Ghobadi, H., Spogli, L., Alfonsi, L., Cesaroni, C., Cicone, A., Linty, N., ... Ca-
498 faro, M. (2020). Disentangling ionospheric refraction and diffraction effects
499 in gnss raw phase through fast iterative filtering technique. *GPS Solut.*, *24*,
500 85. Retrieved from <https://doi.org/10.1007/s10291-020-01001-1> doi:
501 10.1007/s10291-020-01001-1
- 502 Grossmann, A., Lohse, D., & Reeh, H. (1997). Application of extended self-
503 similarity in turbulence. *Phys. Rev. E*, *56*, 5413–5478.
- 504 Groves, K. M., Basu, S., Weber, E. J., Smitham, M., Kuenzler, H., Valladares, C. E.,
505 ... Kend, M. J. (1997). Equatorial scintillation and systems support. *Radio
506 Sci.*, *32*, 2047–2064.
- 507 Hamza, A. M., & St-Maurice, J.-P. (1993). A turbulent theoretical framework
508 for the study of current-driven E region irregularities at high latitudes: Basic
509 derivation and application to gradient-free situations. *J. Geophys. Res.*, *98*,
510 11,587–11,599.
- 511 Jakeman, E., & Tough, R. J. A. (1988). Non-Gaussian models for the statistics of
512 scattered waves. *Adv. in Physics*, *37*, 471–529.
- 513 Jayachandran, P. T., Langley, R. B., MacDougall, J. W., Mushini, S. C.,
514 Pokhotelov, D., Hamza, A. M., ... Carrano, C. S. (2009). Canadian
515 High Arctic Ionospheric Network (CHAIN). *Radio Sci.*, *44*, RS0A03. doi:
516 10.1029/2008RS004046
- 517 Kintner, P. M., Kil, H., Beach, T. L., & de Paula, E. R. (2001). Fading timescales
518 associated with GPS signals and potential consequences. *Radio Sci.*, *36*, 731–
519 743.
- 520 Kintner, P. M., Ledvina, B. M., & de Paula, E. R. (1982). Non-linear evolution
521 of plasma enhancements in the auroral ionosphere, 1. Long wavelength irreg-
522 ularities. *J. Geophys. Res.*, *87*, 144–150. Retrieved from [https://doi.org/
523 10.1029/JA087iA01p00144](https://doi.org/10.1029/JA087iA01p00144) doi: 10.1029/JA087iA01p00144
- 524 Kintner, P. M., Ledvina, B. M., & de Paula, E. R. (2007). GPS and ionospheric
525 scintillations. *Space Weather*, *5*, S09003. Retrieved from [https://doi.org/10
526 .1029/2006sw000260](https://doi.org/10.1029/2006sw000260) doi: 10.1029/2006sw000260
- 527 Kintner, P. M., & Seyler, C. E. (1985). The status of observations and theory of
528 high latitude ionospheric and magnetospheric plasma turbulence. *Space Sci.
529 Rev.*, *41*, 1572–1672.
- 530 Lawrance, A. J. (1991). Directionality and reversibility in time series. *Interna-
531 tional Statistical Review*, *59*, 67–79. Retrieved from [https://www.jstor.org/
532 stable/1403575](https://www.jstor.org/stable/1403575)
- 533 McCaffrey, A. M., & Jayachandran, P. T. (2019). Determination of the refractive
534 contribution to gps phase “scintillation”. *J. Geophys. Res.*, *124*, 1454–1469.
535 Retrieved from <https://doi.org/10.1029/2018JA025759>

- 536 Mezaoui, H., Hamza, A. M., & Jayachandran, P. T. (2015). High-latitude intermit-
 537 tent ionospheric scintillations: Exploring the castaing distribution. *J. Geophys.*
 538 *Res.*, *120*, 6831–6836. doi: 10.1002/2015JA021304
- 539 Meziane, K., Kashcheyev, A., Patra, S., Jayachandran, P. T., & Hamza, A. M.
 540 (2020). Solar cycle variations of gps amplitude scintillation for the polar
 541 region. *Space Weather*, *18*. Retrieved from [https://doi.org/10.1029/](https://doi.org/10.1029/2019SW002434)
 542 [2019SW002434](https://doi.org/10.1029/2019SW002434) doi: 10.1029/2019SW002434
- 543 Mounir, H., Cerisier, J., Berthelier, A., Lagoutte, D., & Begin, C. (1991). The
 544 small-scale turbulent structure of the high-latitude ionosphere arcad-aureol-3
 545 observations. *Ann. Geophys.*, *9*, 725–737.
- 546 Mushini, S. C. (2012). *Charcateristics of scintillating gps signal at high-latitudes*
 547 *during solar minima* (Unpublished doctoral dissertation). University of New
 548 Brunswick, New Brunswick.
- 549 Pagel, C., & Balogh, A. (2002). ntermittency in the solar wind: A comparison be-
 550 tween solar minimum and maximum using ulysses data. *J. Geophys. Res.*, *107*,
 551 1178–1185. doi: 10.1029/2002JA009331
- 552 Priyadarshi, S. (2015). A review of ionospheric scintillation models. *Surv. Geo-*
 553 *physics*, *36*, 295–324. doi: 10.1007/s10712-015-9319-1
- 554 Rino, C. L. (1979). A power law phase screen model for ionospheric scintillation, 1.
 555 weak scatter. *Radio Sci.*, *14*, 81135-1145.
- 556 Rufenach, C. L. (1972). Power-law wavenumber spectrum deduced from ionospheric
 557 scintillation observations. *J. Geophys. Res.*, *77*, 4761–4772. doi: 10.1029/
 558 [JA077i025p04761](https://doi.org/10.1029/JA077i025p04761)
- 559 Sagdeev, R. Z. (1979). The 1976 Oppenheimer lectures: Critical problems in plasma
 560 astrophysics, i. turbulence and nonlinear waves. *Rev. Mod. Phys.*, *51*, 1–9.
- 561 Sato, T., Takao, T., & Maeda, K. (1968). Fully developed turbulent irregularities in
 562 the ionosphere due to cross-field plasma instability. *Radio Sci.*, *3*, 529–534.
- 563 Sosa-Correa, P., Pereira, R. M., Macêdo, A. M. S., Raposo, E. P., Salazar, D. S. P.,
 564 & Vasconcelos, G. L. (2019). Emergence of skewed non-gaussian distributions
 565 of velocity increments in isotropic turbulence. *Phys. Rev. Fluids*, *4*, 064602.
- 566 Taylor, G. I. (1935). Statistical theory of turbulence. In *Proc. R. Soc. Lond., A* (pp.
 567 421–444). doi: 10.1098/rspa.1935.0158
- 568 Taylor, G. I. (1938). The spectrum of turbulence. In *Proc. R. Soc. Lond., A* (pp.
 569 476–490). doi: 10.1098/rspa.1938.0032
- 570 Wernik, A. W., Alfonsi, L., & Materassi, M. (2007). Scintillation modelling using
 571 in situ data. *Radio Sci.*, *42*, RS1002. Retrieved from [https://doi.org/10](https://doi.org/10.1029/2006RS003512)
 572 [.1029/2006RS003512](https://doi.org/10.1029/2006RS003512) doi: 10.1029/2006RS003512
- 573 Weygand, J. M., Kivelson, M. G., Khurana, K. K., Schwarzl, H. K., Walker, R. J.,
 574 Balogh, A., . . . Goldstein, M. L. (2006). Non-self-similar scaling of plasma
 575 sheet and solar wind probability distribution functions of magnetic field fluctu-
 576 ations. *J. Geophys. Res.*, *111*. doi: 10.1029/2006JA011820
- 577 Yeh, K. C., & Liu, C.-H. (1982). Radio wave scintillation in the ionosphere. In *Pro-*
 578 *ceedings of the IEEE* (pp. 324–360).